Detection of body noise with an ultra-sensitive SQUID system

To cite this article: J-H Storm *et al* 2019 *Meas. Sci. Technol.* **30** 125103

View the article online for updates and enhancements.

Detection of body noise with an ultra-sensitive SQUID system

J-H Storm, P Hömmen, N Höfner and R Körber

Physikalisch-Technische Bundesanstalt (PTB), Abbestraße 2-12, 10587 Berlin, Germany

E-mail: rainer.koerber@ptb.de

CrossMark

Abstract

Using an ultra-sensitive single-channel SQUID system an upper limit of 80 aT Hz$^{-1/2}$ for the body noise contribution of the human head in ultra-low-field SQUID-based MRI or MEG is determined. We discuss in detail the various noise contributions which need to be taken into account. Simulations and measurements of conducting phantoms show that presumably residual radio frequency interference cause an increase in the sensor noise at the aT Hz$^{-1/2}$-level and need to be considered. Using a phenomenological approach, the body noise contribution of the human head is determined to 55 aT Hz$^{-1/2}$ for our setup. We also provide simulations of the expected body noise for other sensor geometries.

Keywords: body noise, SQUID, phantom

(Some figures may appear in colour only in the online journal)

1. Introduction

Highly sensitive superconductive quantum interference device (SQUID) systems are extensively used in biomagnetism. In magnetoencephalography (MEG) commercially available multi-channel systems measure the weak magnetic fields generated by ionic currents within the brain [1]. Usually those systems utilise low critical temperature (low-T_c) SQUIDs and show a white noise of about 2 fT Hz$^{-1/2}$. Another application is SQUID-based ultra-low field magnetic resonance imaging (ULF MRI) [2]. Recently, custom-designed single-channel or few-channel SQUID systems with noise figures below 1 fT Hz$^{-1/2}$ have been built [3–6]. Ultimately, thermal noise due to the conducting tissue will be the limiting factor which has been estimated to be around 50 aT Hz$^{-1/2}$ for a typical pick-up coil geometry used in ULF MRI [7].

Thermal noise from a conducting tissue can be observed in high field MRI where it manifests itself as an additional resistance of the loaded MRI coil [8]. In ULF MRI or MEG, body noise has not been the limiting factor so far. However, an ultra-sensitive broadband SQUID system with a white noise of about 150 aT Hz$^{-1/2}$ has been built [9] which should be able to detect body noise contributions directly.

Utilising that particular system, we present measurements of the thermal noise of the human head and conductivity phantoms. The quantitative determination of body noise would offer the ability to measure the effective conductivity of human tissue non-invasively, contact free, and with high bandwidth up to the MHz-range.

2. Materials and methods

2.1. The ultra-sensitive SQUID system

The single-channel SQUID system used in this work is described in detail in [9]. Briefly, a single-stage current sensor low-T_c SQUID with additional positive feedback (APF) [10] and an input coil inductance $L_i = 400$ nH is connected to a first order axial gradiometer with a baseline b of 120 mm and a radius r_p of 22.5 mm. Its inductance L_p was 413 nH and hence close to optimum matching is achieved. The gradient sensitivity, $G_\Phi = \Delta B/(b\,\Phi_{SQ})$, relating the gradient change $\Delta B/b$ to the flux in the SQUID Φ_{SQ}, is given by $G_\Phi = L_{tot}/(M_{in} r_p^2 \pi b)$. The measured mutual inductance between input coil and SQUID M_{in} is 4.0 nH and L_{tot} is the total inductance of the input circuit. For calculating

Table 1. Parameters of the 4-layer cylindrical conductor model with diameter of 200 mm and total height of 150 mm. The temperature is 310 K and the conductivity is homogeneous within anyone layer with L1 being closest to the pick-up coil, values taken from [14].

Layer	Conductivity ($S\,m^{-1}$)	Thickness (mm)
L1: scalp	0.33	2.4
L2: skull	0.008	4
L3: cerebrospinal fluid (CSF)	1.79	1.6
L4: brain matter	0.33	142

G_Φ, L_{tot} was determined as described in [6] and we obtain $G_\Phi = 2.2$ nT/(m Φ_0). The SQUID probe is operated in the custom-built fibre-glass liquid Helium Dewar LINOD2 which features negligible noise. The measurements were performed inside the moderately magnetically shielded room 'Zuse-MSR' of PTB consisting of two layers of μ-metal and one eddy current layer made of copper-plated aluminium [11].

Measurements with the SQUID connected to a dummy pick-up coil with a comparable inductance $L_p = 370$ nH inside a superconducting niobium (Nb) shield were performed to investigate the noise performance in a truly noise-free environment.

2.2. Measurements of thermal noise

For the measurement of the thermal noise emanating from the human head, the dewar was positioned tangentially over the somatosensory cortex of three subjects with a gap of about 1 mm. The resulting distance of the head surface to the bottom loop of the pick-up coil was $\sim$14 mm.

For conducting samples at 295 K, cylindrical phantoms consisting of aqueous solutions of NaCl with conductivities of 4.76 S m^{-1}, 1.774 S m^{-1} and 0.325 S m^{-1} (measued with Mettler Toledo InLab® 731 ISM) were used. The latter corresponds to the average conductivity of the brain when treated homogeneously [12]. The cylinder had a diameter of 130 mm and a height of 115 mm. The distance d to the bottom pick-up loop was varied between 14 and 65 mm. Below, we quote the white noise values and assign the standard deviation derived from the noise power spectra as the measurement uncertainty.

2.3. Simulations of thermal noise

The thermal noise of the physical phantoms described above and two further conductor models at body temperature (310 K) was calculated following the procedure given in [9]. The models consisted of a homogeneous and a 4-layer cylinder, both having a diameter of 200 mm and a total height of 150 mm. The conductivity of the homogeneous cylinder was 0.33 S m^{-1}, the parameters of the 4-layer model are given in table 1. The radius r of a magnetometer pick-up coil and the distance d to the conductor surface were varied from 1 to 50 mm and from 0 to 30 mm, respectively. For small values of r and d this resembles closely a pick-up coil above an infinite planar conductor.

The calculation proceeds by determining the frequency dependent dissipated power $P(f)$ in the sample due to a time harmonic current $I_0 \exp(i2\pi ft)$ in the pick up coil. From $P(f) = I_0^2 Re\{Z(f)\}/2$, the real part of the system impedance $Z(f)$ can be obtained which links the dissipated power in the sample to the voltage noise power per unit bandwidth $S_V(f) = 4k_B T Re\{Z(f)\}$ where k_B is Boltzmann's constant and T is the sample temperature [13]. Using Faraday's law and the pick-up coil area A_p, the magnetic flux density noise of the system is given by:

$$S_{B,\text{sample}}^{1/2}(f) = \frac{\sqrt{4k_B T \cdot 2P(f)}}{2\pi f A_p I_0}. \tag{1}$$

For the calculation of $P(f)$, we restrict our analysis to ohmic contributions induced by the frequency-independent sample conductivity σ and neglect dielectric dissipation governed by the imaginary part of the permittivity ϵ''. The condition $\sigma \gg 2\pi f \epsilon_0 \epsilon''$ is fulfilled in our case as we use a limited frequency range of 80 kHz [15, 16]. A frequency-independent σ and negligible shielding effects result in a white field noise $S_{B,\text{sample}}^{1/2}$.

2.4. The noise budget

A quantitative determination of the thermal body noise requires a detailed knowledge of the individual contributions to the SQUID sensor noise. For an open input coil arrangement inside the superconducting Nb shield, the measured total SQUID flux noise power $S_{\Phi,m}$ is given by:

$$S_{\Phi,m} = S_{\Phi,i} + S_{\Phi,amp} = S_{\Phi,i} + S_{V,amp}/V_\Phi^2, \tag{2}$$

where $S_{\Phi,i}$ is the intrinsic SQUID flux noise and $S_{\Phi,amp}$ are contributions due to the read-out amplifier. $S_{V,amp}$ is the voltage noise of the pre-amplifier and V_Φ is the flux-to-voltage transfer coefficient at the working point. The equivalent flux noise of 47 nΦ_0 Hz$^{-1/2}$ due to the pre-amplifier current noise is negligible owing to the small dynamic resistance R_{dyn} of the SQUID.

The SQUID and the pick-up coil form the sensor and its flux noise $S_{\Phi,sen}$ depends on the total inductance L_{tot} of the input circuit due to screening effects of the bare SQUID inductance L_{gSQ}. The screened SQUID inductance L_{SQ} is given by $L_{SQ} = (1 - k^2 L_i/L_{tot})L_{gSQ}$ [17] where k is the coupling constant between input coil and SQUID. This actually reduces the flux noise when the SQUID is coupled to an inductive load. Using $\epsilon_c = 16k_B T(L_{SQ}C)^{1/2} = S_\Phi/2L_{SQ}$, where C is the junction capacitance, one can deduce $S_\Phi^{1/2} \propto L_{SQ}^{3/4}$.

In the superconducting shield with the SQUID connected to the dummy coil no external noise sources are present. In the MSR environment, the gradiometric pick-up coil suppresses the magnetic noise of the μ-metal chamber $S_{\Phi,\mu}$ and any other far-field environmental contributions $S_{\Phi,env}$ to an insignificant level leading to

$$S_{\Phi,m} = S_{\Phi,sen} + S_{V,amp}/V_\Phi^2 + S_{\Phi,sample}, \tag{3}$$

Table 2. SQUID system parameters for the operation inside a superconducting Nb shield and in the MSR with and without subject. White noise values are quoted and the magnetic flux is given in units of the flux quantum Φ_0.

Parameter	Open input	Dummy coil Nb shield	Gradiometer MSR	Gradiometer MSR + subj.
L_i (nH)	400	400	400	400
$L_p + L_{str}$ (nH)	—	370	413	413
V_Φ (mV/Φ_0)	1.84	1.65	1.06	0.924
$S_{\Phi,amp}^{1/2}$ (nΦ_0 Hz$^{-1/2}$)	217 ± 2	243 ± 2	401 ± 4	463 ± 4
$S_{\Phi,m}^{1/2}$ (nΦ_0 Hz$^{-1/2}$)	673 ± 4	537 ± 4	669 ± 3	766 ± 4
$S_{\Phi,sen}^{1/2}$ (nΦ_0 Hz$^{-1/2}$)	637 ± 5[a]	478 ± 4	535 ± 4	610 ± 4[b]
$S_{B,amp}^{1/2}$ (aT Hz$^{-1/2}$)	—	—	106 ± 1	122 ± 1
$S_{B,m}^{1/2}$ (aT Hz$^{-1/2}$)	—	—	177 ± 1	202 ± 1
$S_{B,sen}^{1/2}$ (aT Hz$^{-1/2}$)	—	—	141 ± 1	161 ± 1[b]

[a] $S_{\Phi,i}^{1/2}$.
[b] $(S_{sen} + S_{sample})^{1/2}$.
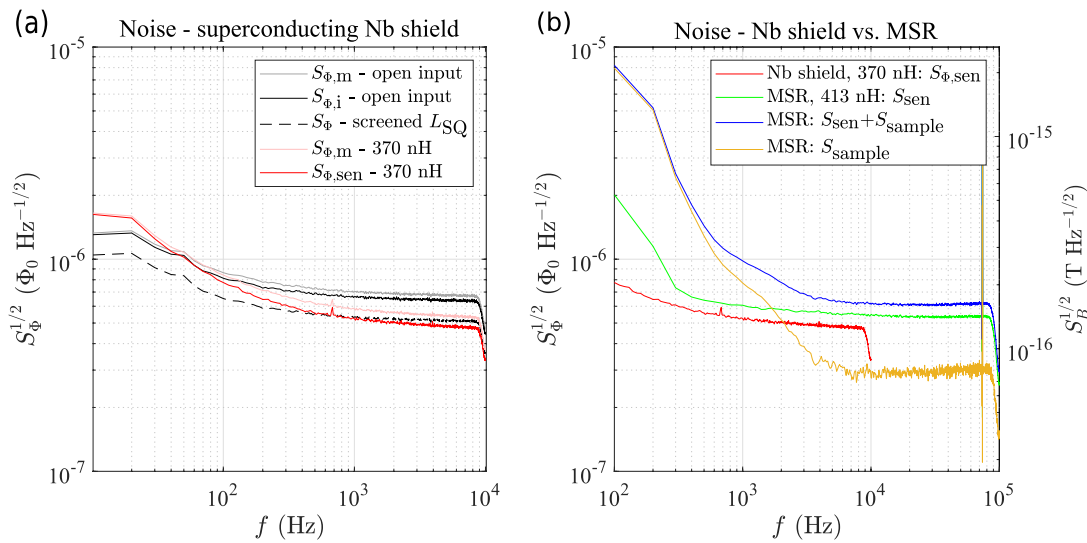
Figure 1. (a) Noise contributions of the SQUID system for the dummy pick-up coil with $L_p = 370$ nH within a superconducting shield (red) and for the open input coil (black) showing the noise decrease due to SQUID inductance screening. The dashed black line is obtained by scaling $S_{\Phi,i}^{1/2}$ as $L_{SQ}^{3/4}$. (b) Comparison of $S_{\Phi,sen}^{1/2}$ (370 nH, red) with the actual gradiometric pick-up coil inside the MSR (green). The similar pick-up coil inductances L_p enable a straight forward comparison as the screening effect is comparable in both cases. *In vivo* measurement showing the sensor noise with the subject and the reference measurement subtracted. Equivalent field noise referred to the bottom pick-up loop of the gradiometer is shown on the right.

where $S_{\Phi,sample}$ is the flux noise power of the sample or subject (if present).

3. Results and discussion

3.1. SQUID system noise performance

The main SQUID system parameters determined for the various conditions are given in table 2. Discussing first the results obtained in the superconducting shield, we also refer to figure 1(a) in which the measured and the intrinsic flux noise $S_{\Phi,m}^{1/2}$ and $S_{\Phi,i}^{1/2}$ of the SQUID with an open input coil are shown. Also depicted is the SQUID sensor noise with the dummy pick-up coil connected. Due to the large V_Φ there is only a small contribution from the read-out electronics and the reduction in flux noise due to SQUID inductance screening

is clearly observed. We determine $S_{\Phi,i}^{1/2} = 637$ nΦ_0 Hz$^{-1/2}$ and $S_{\Phi,sen}^{1/2} = 478$ nΦ_0 Hz$^{-1/2}$ for the open input and with the dummy pick-up coil inside the superconducting shield, respectively. This is in good agreement with $S_\Phi^{1/2} \propto L_{SQ}^{3/4}$ in the white noise regime (compare red and black, dashed line in figure 1(a)). The superconducting input circuit also leads to a screening of the APF coil and consequently to a reduction of the APF gain. As the APF circuit determines V_Φ this is likely the cause of its decrease from 1.84 to 1.65 mV/Φ_0.

If the SQUID system with the gradiometric pick-up coil is operated in the MSR, the measured noise $S_{\Phi,m}^{1/2}$ increases from 537 to 669 nΦ_0 Hz$^{-1/2}$. This is mainly due to a reduction in V_Φ from 1.65 to 1.06 mV/Φ_0 causing a larger contribution of $S_{\Phi,amp}$ (second term in equation (3)).
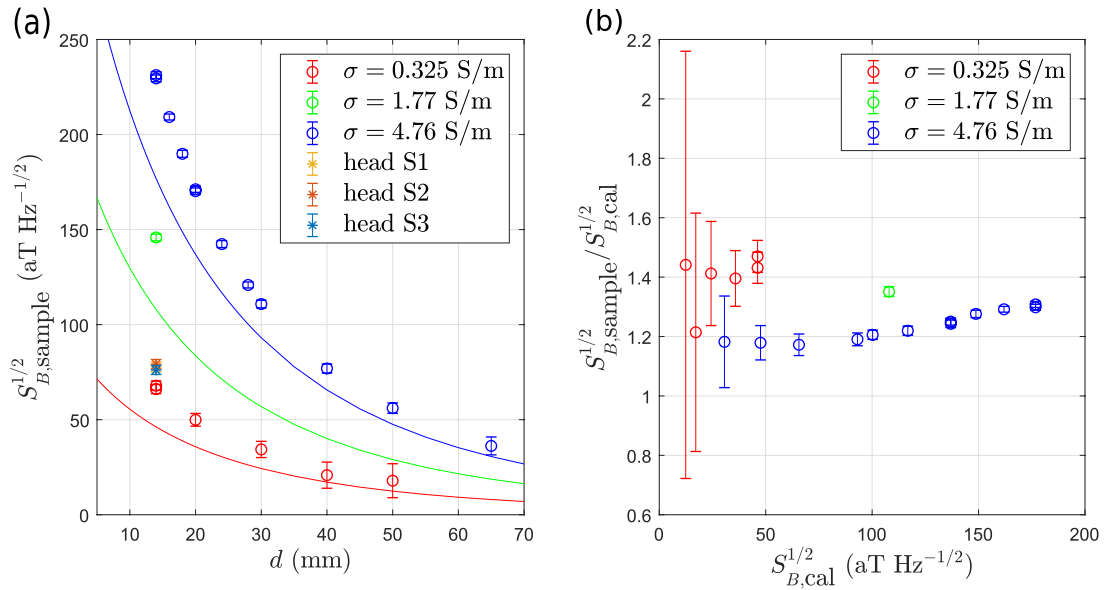
Figure 2. (a) Measured noise $S_{B,\text{sample}}^{1/2}$ (symbols) and calculated noise $S_{B,\text{cal}}^{1/2}$ (solid lines) of conducting cylinders at 295 K with conductivity σ and distance d of the pick-up coil to the solution surface. (b) Ratio $S_{B,\text{sample}}^{1/2}/S_{B,\text{cal}}^{1/2}$ versus $S_{B,\text{cal}}^{1/2}$.

This is accompanied by an increase in the sensor noise $S_{\Phi,\text{sen}}^{1/2}$ from 478 to 535 $\text{n}\Phi_0\ \text{Hz}^{-1/2}$ as shown in figure 1(b). We attribute both effects to residual radio frequency interference (RFI) which has been shown to adversely affect V_Φ and, at the same time, to increase the SQUID noise [18, 19]. The used SQUIDs have integrated *RC* filters on the input circuit with a filter bandwidth of about 100 MHz and consequently some RFI attenuation takes place. A lower filter bandwidth would require a smaller *R* leading to an increased current noise. To avoid degradation of the overall noise performance some compromise must be made, and careful optimisation is required. We did not attempt this at this stage, but this should be addressed in future designs.

3.2. Measurements of thermal noise

In figure 1(b) the sensor noise $S_{\Phi,\text{sen}}^{1/2}$ together with equivalent field noise (referred to the bottom pick-up loop of the gradiometer) for the SQUID system in the MSR with and without one subject is shown. With the subject, activity to about 6 kHz is clearly detectable before the white noise regime with 161 $\text{aT Hz}^{-1/2}$ is reached. Subtracting the reference noise of 141 $\text{aT Hz}^{1/2}$ gives the contribution of the subject. In the white noise regime above 6 kHz this results in $(79 \pm 3)\ \text{aT Hz}^{-1/2}$. The procedure was carried out for all three subjects and the sample noise was found to be similar with $S_{B,\text{sample}}^{1/2} \approx 80\ \text{aT Hz}^{-1/2}$ as shown in figure 2(a).

In figure 2(a) we also present the measured and calculated noise contribution of the conducting cylindrical samples. For large distances d, there is agreement within the accuracy of the measurements, otherwise $S_{B,\text{sample}}^{1/2}$ is larger than $S_{B,\text{cal}}^{1/2}$. In addition, the ratio $S_{B,\text{sample}}^{1/2}/S_{B,\text{cal}}^{1/2}$, shown in figure 2(b), is

not constant but increases with expected noise. This is particularly clear for the phantom with $\sigma = 4.76\ \text{S m}^{-1}$. Hence, subtracting the sensor noise $S_{\Phi,\text{sen}}$ measured without a sample is insufficient and results only in an upper bound of any additional noise $S_{\Phi,\text{sample}}$ as the actual SQUID sensor noise is underestimated in this case.

In explaining these results, it is helpful to examine the correlation between V_Φ and the noise contributions from the samples. In figure 3(a), V_Φ versus the amplifier corrected measured noise corresponding to $(S_{B,\text{sen}} + S_{B,\text{sample}})^{1/2}$ is plotted. We find that V_Φ decreases with increasing sample noise and this is also observed for the *in vivo* measurements.

Attempts to account for this increased sensor noise $S_{B,\text{sen}}$ self-consistently by mixing-down effects of wide-band sample noise beyond the system bandwidth were unsuccessful. As a possible explanation we consider that the residual RFI is modified by the conducting samples causing a stronger interaction with the SQUID system. This would lead to the observed decrease in V_Φ and, at the same time, to an increase in $S_{\Phi,\text{sen}}$.

In the following we use a phenomenological approach to correct for this effect. In figure 3(b) the calculated noise of the sample $S_{B,\text{cal}}$ has been subtracted from the amplifier corrected noise $(S_{B,\text{m}} - S_{B,\text{amp}})$ and is plotted versus the measured V_Φ. The data collapse and we use this as a calibration curve to obtain the true $S_{B,\text{sen}}^{1/2}$ for the *in vivo* measurement. Note, this assumes that the human head and the conductivity samples affect the SQUID performance identically. For the *in vivo* measurements, we determined a $V_\Phi \approx 925\ \mu\text{V}/\Phi_0$. For our geometry of a first order gradiometer with 22.5 mm radius and a distance d to the head of $\sim$14 mm, this gives a corrected sensor noise of $S_{B,\text{sen}}^{1/2} \approx 150\ \text{aT Hz}^{-1/2}$ and a corrected sample or body noise of $S_{B,\text{sample}}^{1/2} \approx 55\ \text{aT Hz}^{-1/2}$.
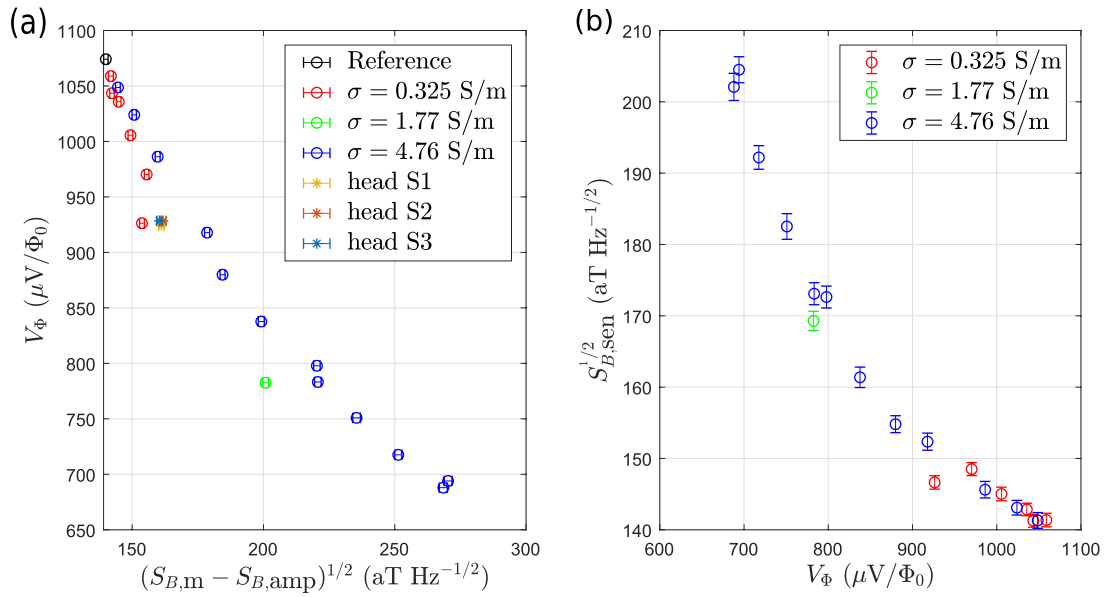
Figure 3. (a) V_Φ decreases with increasing noise of the samples. (b) Subtraction of $S_{B,cal}$ from $(S_{B,m} - S_{B,amp})$ gives the true $S_{B,sen}$ and is used as a calibration curve.
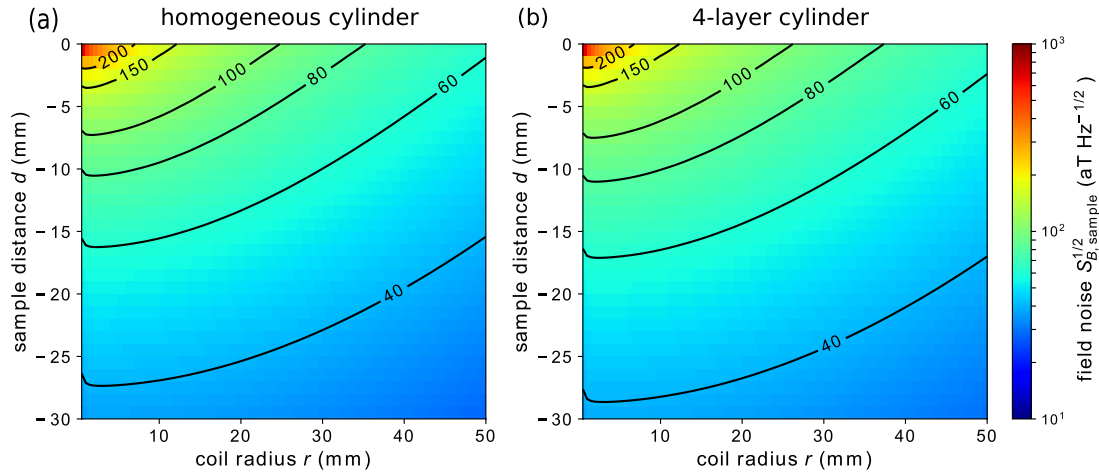
Figure 4. Simulation of the magnetic field noise as detected by a magnetometer pick-up loop with radius r in dependence of the distance d to the sample surface following the procedure described in section 2.3. (a) homogeneous cylinder with $\sigma = 0.33$ S m^{-1} and (b) 4-layer conductor model. Body temperature (310 K) was assumed in both cases.

3.3. Simulation of thermal noise

The results of the simulations of the expected sample noise from the two conductor models are shown in figure 4. Here, we present the calculated field noise for a magnetometer pick-up coil with radius r and a distance d to volume conductor surface. We note that there is only a small quantitative difference in $S_{B,sample}^{1/2}$ between the two conductor models and for our setup with $d = 14$ mm and $r = 22.5$ mm we obtain 57 and 59 aT Hz$^{-1/2}$ for the homogeneous and the 4-layer model, respectively. Those values are very close to the experimental result. For typical MEG systems with a warm-cold distance of more than 30 mm and pick-up coil sizes in the cm-range, the noise would be below 40 aT Hz$^{-1/2}$. Also, a point sensor on top of the surface would detect about 500 aT Hz$^{-1/2}$. It is interesting to apply these results to on-scalp MEG as it is envisaged by the use of optically pumped magnetometers [20, 21]

or high-T_c SQUIDs [22]. The current noise level of a few fT Hz$^{-1/2}$ of these technologies appears to render thermal noise negligible in this case.

4. Conclusion

Using an ultra-sensitive single-channel SQUID system we were able to obtain an upper limit of the body noise contribution of about 80 aT Hz$^{-1/2}$ which is a function of sample and pick-up coil geometry. By performing detailed phantom measurements we found that for our SQUID system the sensor noise S_{sen} is increased and the flux-to-voltage coefficient V_Φ is decreased if a conducting sample is present. We consider interaction between the conducting samples and residual RFI could be responsible for this behaviour. If this effect is unaccounted for, the underestimation of the SQUID noise leads to a too high sample noise and prevents

a quantitative determination of the effective conductivity of a physiological sample. Using a phenomenological approach to quantify S_{sen} we obtained a body noise of the human head of 55 aT Hz$^{-1/2}$. As the performance of SQUID systems is expected to be improved by incorporating for instance SQUIDs with sub-micrometer sized junctions [23] the ultimate limit of body noise could soon be reached. This should enable the contact-free and wide-band determination of the effective conductivity of human tissue.

Acknowledgments

ORCID iDs

R Körber ● https://orcid.org/0000-0001-7052-5134

References

[1] Körber R *et al* 2016 SQUIDs in biomagnetism: a roadmap towards improved healthcare *Supercond. Sci. Technol.* **29** 113001

[2] Kraus R, Espy M, Magnelind P and Volegov P 2014 *Ultra-Low Field Nuclear Magnetic Resonance* (Oxford: Oxford University Press)

[3] Clarke J, Hatridge M and Mößle M 2007 SQUID-detected magnetic resonance imaging in microtesla fields *Annu. Rev. Biomed. Eng.* **9** 389–413

[4] Zotev V S, Matlashov A N, Volegov P L, Urbaitis A V, Espy M A and Kraus R H Jr 2007 SQUID-based instrumentation for ultralow-field MRI *Supercond. Sci. Technol.* **20** S367

[5] Fedele T, Scheer H, Burghoff M, Curio G and Körber R 2015 Ultra-low-noise EEG/MEG systems enable bimodal non-invasive detection of spike-like human somatosensory evoked responses at 1 kHz *Physiol. Meas.* **36** 357–68

[6] Storm J-H, Drung D, Burghoff M and Körber R 2016 A modular, extendible and field-tolerant multichannel vector magnetometer based on current sensor SQUIDs *Supercond. Sci. Technol.* **29** 094001

[7] Myers W, Slichter D, Hatridge M, Busch S, Mößle M, McDermott R, Trabesinger A and Clarke J 2007 Calculated signal-to-noise ratio of MRI detected with SQUIDs and Faraday detectors in fields from 10 μT to 1.5 T *J. Magn. Reson.* **186** 182–92

[8] Harpen M D 1987 Sample noise with circular surface coils *Med. Phys.* **14** 616

[9] Storm J-H, Hömmen P, Drung D and Körber R 2017 An ultra-sensitive and wideband magnetometer based on a superconducting quantum interference device *Appl. Phys. Lett.* **110** 072603

[10] Drung D, Assmann C, Beyer J, Kirste A, Peters M, Ruede F and Schurig T 2007 Highly sensitive and easy-to-use SQUID sensors *Appl. Supercond. IEEE Trans.* **17** 699–704

[11] Voigt J, Knappe-Grüneberg S, Gutkelch D, Haueisen J, Neuber S, Schnabel A and Burghoff M 2015 Development of a vector-tensor system to measure the absolute magnetic flux density and its gradient in magnetically shielded rooms *Rev. Sci. Instrum.* **86** 055109

[12] Hämäläinen M, Hari R, Ilmoniemi R J, Knuutila J and Lounasmaa O V 1993 Magnetoencephalography—theory, instrumentation, and applications to noninvasive studies of the working human brain *Rev. Mod. Phys.* **65** 413–97

[13] Callen H B and Welton T A 1951 Irreversibility and generalized noise *Phys. Rev.* **83** 34–40

[14] Miranda P C, Mekonnen A, Salvador R and Ruffini G 2013 The electric field in the cortex during transcranial current stimulation *NeuroImage* **70** 48–58

[15] Gabriel S, Lau R W and Gabriel C 1996 The dielectric properties of biological tissues: II. Measurements in the frequency range 10 Hz to 20 GHz *Phys. Med. Biol.* **41** 2251–69

[16] Gabriel S, Lau R W and Gabriel C 1996 The dielectric properties of biological tissues: III. Parametric models for the dielectric spectrum of tissues *Phys. Med. Biol.* **41** 2271–93

[17] Clarke J and Braginski A I 2004 *The SQUID Handbook* vol 1 (New York: Wiley)

[18] Ishikawa N, Nagata K, Sato H, Kasai N and Kiryu S 1993 Effect of RF interference on characteristics of DC SQUID system *IEEE Trans. Appl. Supercond.* **3** 1910–3

[19] Koch R H, Foglietti V, Rozen J R, Stawiasz K G, Ketchen M B, Lathrop D K, Sun J Z and Gallagher W J 1994 Effects of radio frequency radiation on the dc SQUID *Appl. Phys. Lett.* **65** 100–2

[20] Iivanainen J, Stenroos M and Parkkonen L 2017 Measuring MEG closer to the brain: performance of on-scalp sensor arrays *NeuroImage* **147** 542–53

[21] Boto E *et al* 2018 Moving magnetoencephalography towards real-world applications with a wearable system *Nature* **555** 657–61

[22] Pfeiffer C, Andersen L M, Lundqvist D, Hämäläinen M, Schneiderman J F and Oostenveld R 2018 Localizing on-scalp MEG sensors using an array of magnetic dipole coils *PLoS One* **13** e0191111

[23] Schmelz M, Zakosarenko V, Schönau T, Anders S, Kunert J, Meyer M, Meyer H-G and Stolz R 2017 A new family of field-stable and highly sensitive SQUID current sensors based on sub-micrometer cross-type Josephson junctions *Supercond. Sci. Technol.* **30** 074010